Inorganic Chemistry

pubs.acs.org/IC Article

Photochemical CO_2 Reduction by a Postsynthetically Modified Zr-MOF

Rosmi Reji, Juan P. Vizuet, Xiaoli Yan, Biki K. Behera, Xin Zheng, Matthew Klenk, Nicholas P. Weingartz, George T. Kostopoulos, Lin X. Chen, Peter Zapol, Neeraj Agarwal, Eliu Huerta, Murat Keceli, Santanu Chaudhuri, and Ksenija D. Glusac*

Cite This: *Inorg. Chem.* 2025, 64, 18304−18315 Read Online

ACCESS | Metrics & More | Article Recommendations | Supporting Information

ABSTRACT: Metal−organic frameworks are an excellent platform for photochemical CO_2 reduction into valuable chemicals. Herein, we report the synthesis and photocatalytic behavior of Ru@MOF-808, a Zr-based MOF, modified with a Ru-polypyridyl complex. The postsynthetic modification was achieved using solvent-assisted incorporation of bipyridine−carboxylate ligands onto the nodes of the MOF-808, followed by the coordination of Ru(II)-terpyridine moiety. A thorough characterization including ^{1}H NMR, diffuse reflectance UV/vis, X-ray absorption spectroscopy and gas adsorption studies, combined with DFT calculations, provides strong support for efficient incorporation of the molecular Ru-complex at the loading of one Ru center per node. In the presence of a strong sacrificial reductant BIH, Ru@MOF-808 was found to catalyze the photochemical reduction of CO_2 into a mixture of CO and formate ion. When compared to the homogeneous model catalyst $Ru(tpy)(bpy)^{2+}$, Ru@MOF-808 was found to exhibit higher formate yields. To explain these formate enhancements, we propose a mechanism that involves CO_2 capture at the MOF nodes to form Zr-bicarbonate species, which further react in a hydride transfer reaction with photogenerated Ru−H donor, thereby outperforming molecular catalysts in $HCOO^-$ production. Overall, the results presented in this work indicate the potential of Zr-based MOFs in integrating CO_2 capture with its photochemical conversion to desired products.

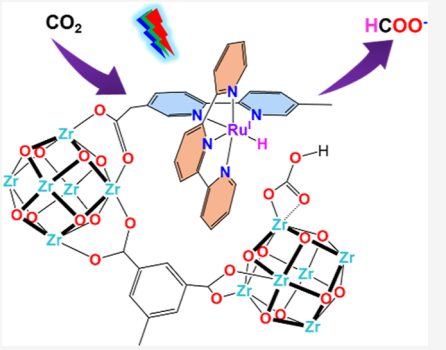

1. INTRODUCTION

Artificial photosynthesis, a process in which carbon dioxide is photochemically reduced to value-added products, represents an important approach toward carbon dioxide upcycling using renewable energy sources.[1−3] Metal−organic frameworks (MOFs), modified with molecular catalysts and chromophores, are excellent "molecular photoreactors" for photochemical CO_2 reduction.[4] The molecular chromophores and catalysts are usually introduced into MOFs using postsynthetic methods that rely on the node functionalization with carboxylate-functionalized molecules,[5−7] metal coordination to bipyridine-based ligands,[8−10] or electrostatic interactions between the oppositely charged MOF and the molecular catalyst.[11,12] The immobilization of the catalysts into MOFs often increases their stability by preventing undesired decomposition pathways.[11,13−15] Furthermore, the MOF cavity provides three-dimensional scaffold for dynamic orientation of complex bimetallic catalytic motifs for target transformation.[6,16] The MOF scaffold also enables the integration of chromophores and catalysts in close proximity, greatly enhancing the photocatalytic performance relative to the homogeneous analogs.[10] The chemical tunability of molecular catalysts within the MOF enables efficient product selectivity enhancements. For example, Cu-based catalysts have been shown to selectively produce either carbon monoxide or formate ion, depending on the hydrogen-bonding stabilization effects provided by the ligand.[9] The MOFs with different pore sizes can affect photocatalytic performance via their different abilities to host chromophores and catalysts of different sizes.[17,18] While C1 products, such as CO, formate or methane, are usually formed, recent studies have shown that acetic acid can be formed using a Ce-based MOF.[8] Recent studies have also shown that integrated CO_2 capture and conversion can be achieved using ionic liquids.[19]

Ru-polypyridyl complexes with one or more labile ligands have been shown to catalyze electrochemical carbon dioxide reduction.[20] The reaction most often produces two-electron reduced products, CO and formate.[5,19,21−27] The electron accumulation involves two ligand-centered reductions,[21] and the sequence of chemical and electron transfer steps can be controlled using steric effects.[23,24] The proposed mechanism

Received: June 7, 2025
Revised: August 15, 2025
Accepted: August 19, 2025
Published: August 29, 2025

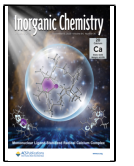

https://doi.org/10.1021/acs.inorgchem.5c02600
Inorg. Chem. 2025, 64, 18304−18315

for CO formation involves the reaction of two-electron-reduced complex with CO_2 to form the metal-bound CO_2 adduct, which is further reduced, causing the loss of O^{2-} dianion and the formation of metal-bound carbon monoxide (M-CO).[21,26−28] The O^{2-} dianion is transferred either to protons to form water[26,27] or to CO_2 molecule to form the CO_3^{2-} dianion.[28,29] It was also found that O^{2-} transfer in the reduction of CO_2 to CO and CO_3^{2-} was facilitated by flexible ligation of the methyl-substituted bipyridine ligand and the formation of a 5-membered metallacycle.[28] In the case of formate production, two different mechanisms have been proposed. One involves the reaction of OH^- ions with M-CO intermediate to yield M-COOH adduct from which the formate ion is released.[26,27] A more commonly accepted mechanism involves the insertion of CO_2 into the Ru−H complex formed upon the protonation of the doubly reduced molecular precursor,[30] which is consistent with previous findings involving reactions of CO_2 with Ru-based hydrides.[31−34] The reduction that goes beyond the two-electron pathway, such as methanol has been demonstrated to occur from M-CO adduct at low temperatures using either electrochemical methods[35] or the utilization of recyclable organic hydrides.[36]

The photocatalytic carbon dioxide reduction by Ru-tpy based complexes have been hampered by their short-lived excited states.[37,38] While many Ru-based compounds exhibit long-lived triplet metal-to-ligand charge transfer (^{3}MLCT) states, the excited states of Ru-tpy complexes are short-lived (few hundred nanoseconds) due to the presence of close-lying triplet metal-centered (^{3}MC) states which tend to undergo rapid nonradiative decay to the ground state.[37] For this reason, Ru-tpy catalysts are often combined with light-harvesting chromophores to enable photocatalytic CO_2 reduction.[16,30] Despite their short-lived excited states, Ru-tpy complexes has been applied in direct photochemical reactions involving either photogeneration of a Ru−H complex[39] or photochemical reduction of CO_2.[40,41]

In this study, we report the synthesis of Ru@MOF-808, a MOF with benzene-1,3,5-tricarboxylate ligands and Zr-based nodes that are postsynthetically modified with Ru(tpy)(bpy)-ACN^{2+} units (Scheme 1, tpy-terpyridine, bpy-5,5′-dimethyl-2,2′-bipyridine). Characterization revealed that the Ru-coordinated moieties in Ru@MOF-808 are structurally analogous to the molecular complex $Ru(bpy)(tpy)^{2+}$. Additionally, incorporating these moieties into MOF-808 at a loading of one Ru center per Zr node reduces the material's surface area by half. We investigated the photocatalytic CO_2 reduction activity of Ru@MOF-808 using different sacrificial electron donors and found that, in the presence of a strong reductant, conversion to C_1 products—CO and formate—occurs. Under photocatalytic conditions, Ru@MOF-808 generates more formate compared to the $Ru(tpy)(bpy)ACN^{2+}$ model complex, which favors CO production. These results suggest that the MOF scaffold plays a key role in steering product distribution. Building on this study and our previous findings that CO_2 insertion into Zr nodes activates bound bicarbonates toward formate formation, we propose a mechanism involving photochemical reduction via hydride transfer between Zr-bound bicarbonate and a photogenerated Ru-hydride intermediate. This work highlights the ability of MOF-based nodes to enable cooperative catalysis by integrating substrate-binding sites with reduction-active moieties (an early version of this manuscript has been deposited in *ChemRxiv*[42]).

Scheme 1. Schematic Illustration of Photocatalytic CO_2 Reduction into CO and $HCOO^-$ by Ru@MOF-808

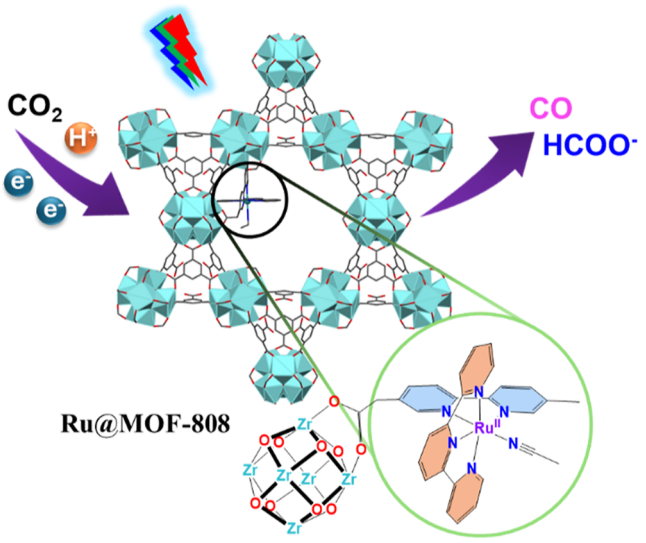

2. EXPERIMENTAL SECTION

2.1. Methods. *2.1.1. Synthesis.* A detailed descriptions of material synthesis, including molecular catalyst-Ru(tpy)(bpy)-ACN, MOF-808, and bpy@MOF-808 used in this study, are provided in the Supporting Information (Section S1).

2.1.2. Synthesis of Ru@MOF-808. The coordination of $[Ru^{II}(tpy)(ACN)_3][PF_6]_2$ to bpy@MOF-808 (2 bpy/node) was achieved using a previously reported method. bpy@MOF-808 (100 mg, 0.06 mmol) and $[Ru^{II}(tpy)(ACN)_3][PF_6]_2$ (44.8 mg, 0.06 mmol) were mixed in a 10 mL dry ethanol/toluene (1:1) solvent mixture. The suspension was outgassed, sealed, and heated at 90 °C for 24 h. After the reaction, the purple product was filtered and washed three times with ethanol and five times with acetonitrile to remove excess $[Ru^{II}(tpy)(ACN)_3][PF_6]_2$. Anal. Calcd for Ru@MOF-808 = $Zr_6O_4(OH)_4(C_9H_3O_6)_2(C_{13}H_{11}O_2N_2)_{1.5}(RuC_{17}H_{14}N_4)_{0.8}(C_2F_3O_2)_4(OH)_1{\cdot}8H_2O$ Elemental analysis: Zr, 22.3%; Ru, 3.29%; C, 28.89%; N, 3.53%; H, 2.77%; F, 9.28%. Found: Zr, 22.9%; Ru, 3.33%; C, 27.7%; N, 3.63%; H, 2.71%; F, 8.93%.

2.1.3. Material Characterization. Materials used in this study are characterized using ^{1}H NMR, pXRD, diffuse reflectance spectroscopy, gas adsorption studies and X-ray absorption studies. Details regarding these characterizations can be obtained from the Supporting Information.

2.1.4. Photocatalytic CO_2 Reduction Studies. A 50 mL photoreactor was equipped with a stir bar and was charged with ACN/H_2O (16 mL, 39:1), Ru@MOF-808 (3 mg, 0.73 μmol Ru-sites) and 0.05 M BIH (1,3-dimethyl-2-phenyl-2,3-dihydro-1*H*-benzo[*d*]imidazole). The mixture was sparged with CO_2 for 40 min, followed by an additional 10 min for the headspace of the reactor. The photoreactor was placed between two of the white light sources (120 W LED Flood light). The illumination was performed for 48 h. At an interval of 4 h, the gas products and liquid products were collected and analyzed using gas and ion chromatography, respectively.

2.2. Computational Details. Detailed description of computational methods adopted for DFT simulation on surface area calculations, close contact search, free energy calculations and classical molecular dynamics are included in the Supporting Information.

https://doi.org/10.1021/acs.inorgchem.5c02600
Inorg. Chem. 2025, 64, 18304−18315

Scheme 2. Synthesis of Ru@MOF-808[a]

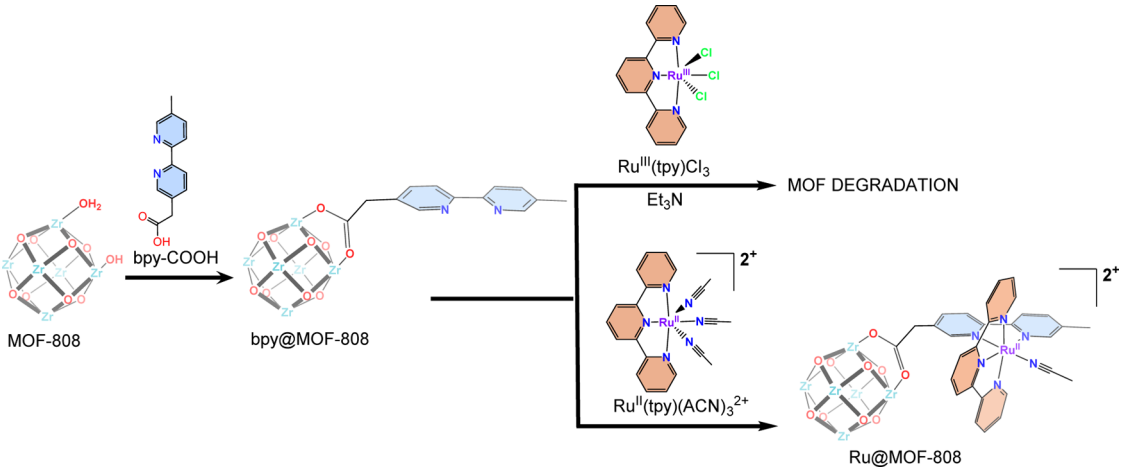

[a]The post-synthetic modification of MOF-808 with carboxylated bpy precursor afforded bpy@MOF-808. While the synthesis of Ru@MOF-808 did not proceed when Ru(III) precursor and triethylamine were used, the reaction was successful when Ru(II) reagent was employed.

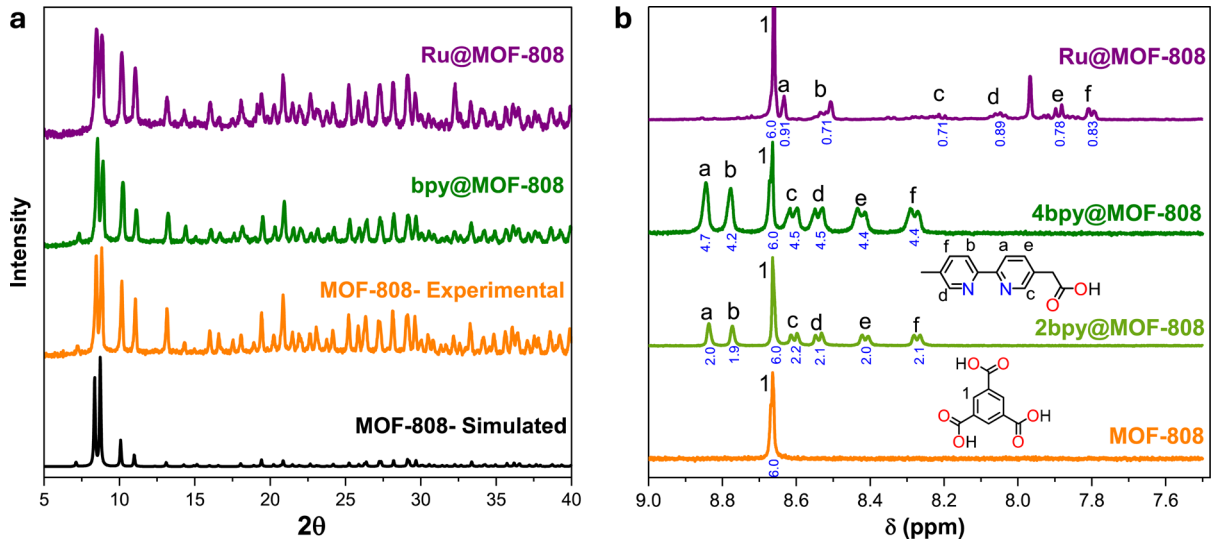

Figure 1. (a) pXRD of MOF-808, bpy@MOF-808 (2bpy/node) and Ru@MOF-808. The simulated pXRD was obtained from using the structure obtained using single-crystal XRD.[43] (b) ^{1}H NMR spectra of D_2O solutions after the MOF digestion (MOF-808 and bpy@MOF-808 were acid-digested, while Ru@MOF-808 was base-digested).

3. RESULTS AND DISCUSSION

3.1. Synthesis and Characterization of Ru@MOF-808.

MOF-808 was selected for this study due to the high stability of Zr-based MOFs.[43] Furthermore, the modulator molecules can be readily removed from the 6-connected Zr_6 node, resulting in open sites that can serve as anchoring points for a variety of molecules. The MOF-808 cavity (~16 Å) is constructed by the connection of tetrahedrons formed by four different Zr_6 nodes, and this cavity can be accessed through windows formed by six tetrahedrons (~10 Å). The synthesis of Ru@MOF-808 was achieved by a two-step process, as shown in Scheme 2. First, the carboxylated ligand bpy-COOH was grafted onto the modulator-free nodes of MOF-808 using solvent-assisted ligand incorporation.[7] Interestingly, the reaction between the resulting bpy@MOF-808 and Ru(III)(tpy)Cl_3 did not yield the desired Ru@MOF-808 adduct. This lack of reactivity contrasts with the model compound, which readily forms the Ru(II)(tpy)$(bpy)^{2+}$ complex under similar conditions. We hypothesize that this difference in reactivity is due to the use of triethylamine (as a reducing agent for Ru^{III} to Ru^{II} conversion) which caused MOF degradation at elevated temperatures. To overcome this challenge, we synthesized Ru@MOF-808 using the [Ru(II)-(tpy)$(ACN)_3$][PF_6]$_2$ complex as a precursor (synthesis and characterization of precursors are described in Supporting Information, Section S1).

The crystallinity of the samples remained unperturbed by the postsynthetic modifications, as confirmed using powder X-ray diffraction shown in Figure 1a. Different loadings of bpy ligands per node in MOF-808 were achieved by varying the concentration of bpy-COOH (details in the Supporting Information). The ^{1}H NMR spectra of acid-digested bpy@MOF-808 samples with different bpy loadings are shown in Figure 1b. The MOF-808 ligand, benzene tricarboxylic acid, exhibits a single peak in the aromatic region at 8.66 ppm, which was used as a reference signal to evaluate the amount of bpy-COOH loading (integration was set to a value of 6, since there are two tricarboxylic acid ligands per Zr-node in MOF-

https://doi.org/10.1021/acs.inorgchem.5c02600
Inorg. Chem. 2025, 64, 18304−18315

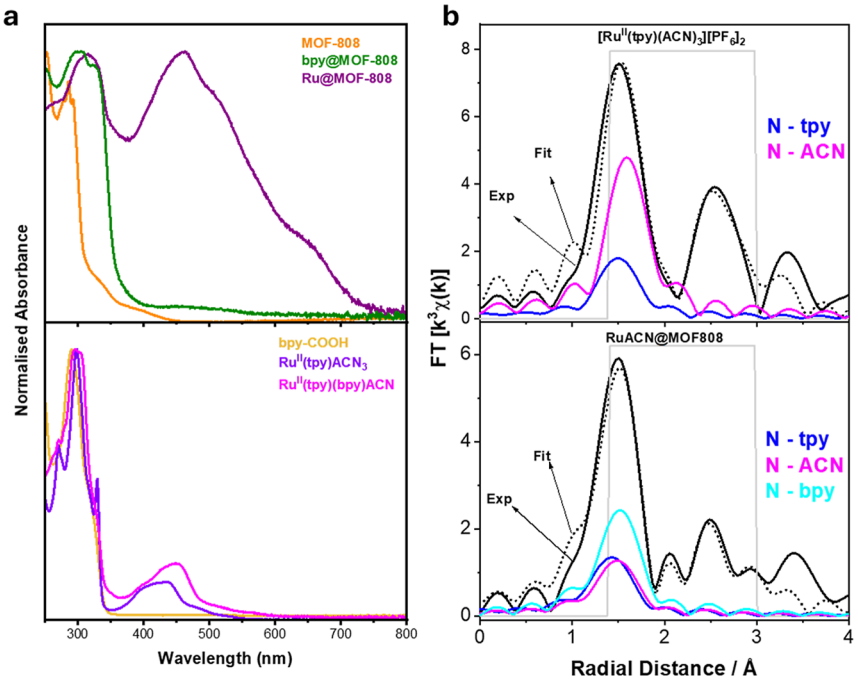

Figure 2. (a) Normalized UV−vis absorption spectra of solid MOF samples (top) and Ru-model compounds in acetonitrile (bottom). (b) Ru K-edge EXAFS data and associated fitting of $[Ru^{II}(tpy)ACN_3][PF_6]$ (top) and Ru@MOF-808 (bottom).

808). The integration of NMR peaks associated with bpy-COOH in the 8.2−9 ppm range indicates that a loading of either approximately two or four bpy units per Zr-node was achieved. The bidentate geometry of bound bpy-COOH is assumed based on previous studies supporting this binding motif.[44,45] The quantification of Ru@MOF-808 was also achieved using ^{1}H NMR of digested samples. In this case, the samples were digested using basic conditions because the acid digestion generated paramagnetic Ru(III) species that made NMR measurements challenging. The ^{1}H NMR of the base-digested Ru@MOF-808 indicates that the bpy-COOH loading decreases after the reaction of bpy@MOF-808 with Ru(II)-$(tpy)(ACN)_3^{2+}$ to a value of less than one bpy ligand per node (Figure 1b). Thus, we conclude that Ru@MOF-808 contains less than one Ru-complex per node, and this result is consistent with the elemental analysis (ICP-OES analysis indicates 0.8 Ru centers per node, Supporting Information, Section 1) and the gas adsorption experiments discussed below.

The spectroscopic characterization of postsynthetically modified MOF-808 was achieved using UV−vis reflectance and X-ray absorption (XAS) (Figure 2). The solid-state UV/vis reflectance data of bpy@MOF-808 and Ru@MOF-808 also indicate that the postsynthetic modification was successful (Figure 2a). The UV/vis diffuse reflectance of MOF-808 exhibits a feature at 270 nm that is associated with the node-centered electronic transitions.[46] This feature is red-shifted in bpy@MOF-808, which is consistent with the presence of additional π, π^* electronic transitions associated with the bpy unit. The UV/vis absorption spectrum of bpy-COOH in acetonitrile exhibits a peak in a similar spectral region, confirming the presence of bpy units in bpy@MOF-808. The UV/vis reflectance of Ru@MOF-808 exhibits an additional peak in the visible region at 462 nm. This feature is associated with the ^{1}MLCT transition from Ru-centered d-orbitals to π^* tpy or bpy-COOH ligand orbitals. The Ru → tpy ^{1}MLCT feature is expected to appear at 450 nm, based on the UV/vis absorption spectra of $Ru(tpy)(ACN)_3^{2+}$ and Ru(tpy)(bpy)-ACN^{2+} in acetonitrile shown in Figure 2a (synthetic details on $Ru(tpy)(bpy)ACN^{2+}$ are provided in Supporting Information, Section S1). Analogous complexes have been shown computationally to exhibit Ru → tpy ^{1}MLCT transition in this spectral region.[37] The carboxylated bpy-COOH ligand in Ru@MOF-808 is more electron-withdrawing than 5,5′-dimethyl-2,2′-bipyridine present in the $Ru(tpy)(bpy)ACN^{2+}$ model compound. Thus, the lowest energy transition in Ru@MOF-808 may be associated with the Ru → bpy-COOH rather than Ru → tpy transition. This difference in lowest energy transitions may explain the observed red-shift of the absorption spectrum of Ru@MOF-808 relative to that of $Ru(tpy)(bpy)ACN^{2+}$. To further confirm that the Ru-complex coordinates to bpy-COOH, we attempted to coordinate the $Ru(tpy)(ACN)_3^{2+}$ precursor to MOF-808 and this sample showed no significant changes in the UV/vis spectra, showcasing the need for the bpy groups to attach the Ru complex Figure S5.

A comparison of Ru K-edge EXAFS data for Ru(tpy)-$(ACN)_3^{2+}$ and Ru@MOF-808 provides evidence for the coordination of the Ru precursor to the bpy units inside MOF-808 (Figure 2b). The first scattering shells of both complexes, which dominate the intensity of the EXAFS spectra up to R = 2 Å, are relatively similar. The signal consists of a dominant peak at a radial distance of 1.5 pm and is consistent with the presence of six coordinating nitrogen atoms in both samples. The main difference between the two EXAFS patterns is at a radial distance of 2.5 pm, where the $Ru(tpy)(ACN)_3^{2+}$ precursor exhibits a much stronger signal. The second shell scattering fit of the experimental data starting from a DFT-calculated structure reveals that the 2.5 pm peak arises due to the multiple scattering pathway (forward scattering) associated with the carbon atoms in linear acetonitrile and polypyridyl ligands (details in Supporting Information, Section S2.2).[47,48] The presence or absence of forward scattering is therefore used here as the distinguishing characteristic between the

https://doi.org/10.1021/acs.inorgchem.5c02600
Inorg. Chem. 2025, 64, 18304−18315

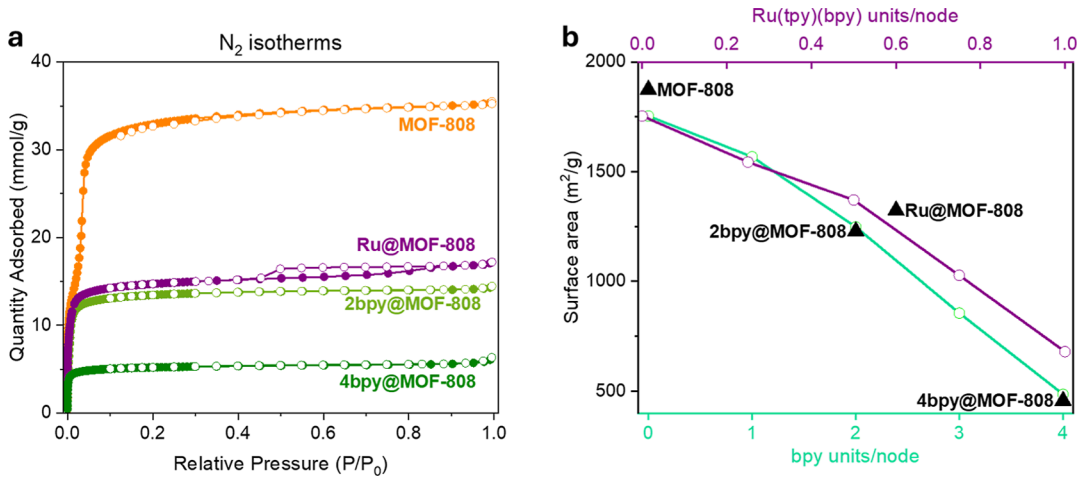

Figure 3. (a) N_2 adsorption−desorption isotherm at 77 K on MOF-808, Ru@MOF-808, 2bpy@MOF-808, and 4bpy@MOF-808. (b) Comparison between experimental (▲) and calculated (○) surface area for MOF-808, 2bpy@MOF-808, 4bpy@MOF-808, and Ru@MOF-808 as a function of bpy unit per node (bottom *x*-axis) and Ru(tpy)(bpy) unit (top *x*-axis).

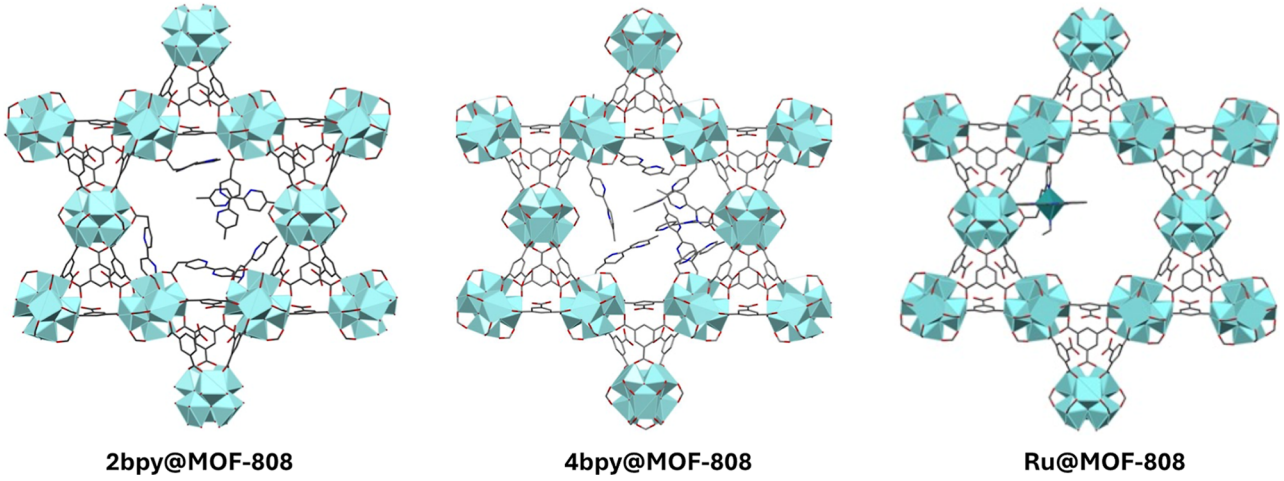

Figure 4. Structures for MOF-808 modified with 2bpy, 4bpy and Ru(tpy)(bpy)ACN^{2+} simulated using Vienna ab initio simulation package (VASP) using projected augmented wave (PAW) formalism.

complexes. In $Ru(tpy)(ACN)_3^{2+}$, the presence of three linear acetonitrile groups results in a particularly strong second shell signal. When two acetonitrile groups are displaced in favor of the nonlinear bpy ligand to obtain Ru@MOF-808, we observe a significant decrease in the second shell intensity. The decreased scattering amplitude indicates the removal of two ACN and the subsequent binding of the bpy cyclometallating ligand.

The porosity of postsynthetically modified MOFs was evaluated by measuring the nitrogen adsorption isotherms for the four MOF samples (Figure 3a). All MOFs exhibited type I isotherms with a steep increase in adsorbed gas at low partial pressures, consistent with nanometer-sized pores. The experimental data were fitted using the BET model to derive the surface area of each material and the resulting values are plotted in Figure 3b. As expected, the surface area of MOF-808 (1874 m^2/g) is higher than that of bpy@MOF-808 (1228 m^2/g for the sample with 2bpy/node and 457 m^2/g for 4bpy/node). The surface area of Ru@MOF-808 (1323 m^2/g) was higher than that of the precursor bpy@MOF-808 with 2bpy/node. This result is consistent with the NMR results shown in Figure 1b that illustrate that half of the bpy units are removed from the MOF during the reaction with $Ru(tpy)(ACN)_3^{2+}$. It is interesting that Ru@MOF-808 exhibits an adsorption/desorption hysteresis, and this behavior is likely associated with the presence of very small pores within Ru@MOF-808 where nitrogen accessibility is restricted at 77 K and equilibrium is not achieved within the equilibration time of the experiment.[49]

To further understand the changes observed in experimental adsorption isotherms, we performed molecular dynamics simulations for MOF-808 with a varying number of bpy-COOH units per node (computational details described in Section S4 of the Supporting Information). The optimized structures of bpy@MOF-808 containing either two or four bpy/node demonstrate our intuition that the kinetics of bpy ligand attachment to the surface of the node may be sterically hindered as the synthesis progresses (Figure 4). This implies not all surface sites are converted from activated H_2O/OH to bpy-COOH. In addition, the simulation cell of MOF-808 possesses an open pore volume of ∼70%, which goes down to 40% for 2bpy@MOF-808 and 19% for 4bpy@MOF-808. This result is consistent with experimentally obtained values for surface area as shown in Figure 3b. In the case of Ru@MOF-808, a linear drop in the percentage of the open pore volume is

https://doi.org/10.1021/acs.inorgchem.5c02600
Inorg. Chem. 2025, 64, 18304−18315

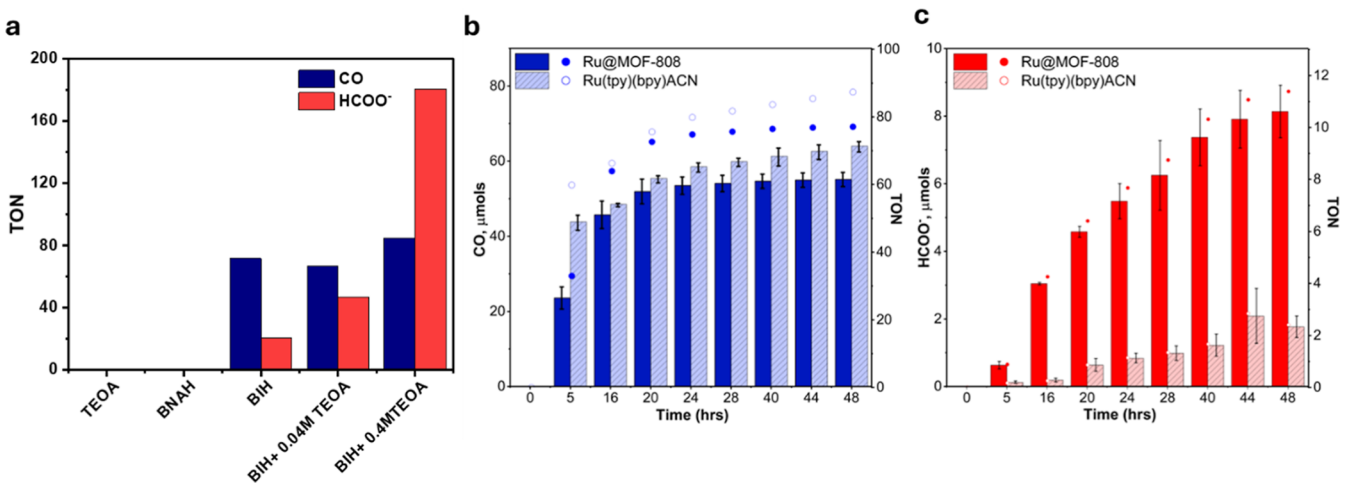

Figure 5. (a) Photochemical CO_2 reduction studies using Ru@MOF-808 under different experimental conditions. (b) CO formation (c) $HCOO^-$ generation as a function of time during photocatalytic CO_2 reduction by Ru@MOF-808 and $Ru(tpy)(bpy)ACN^{2+}$ in the presence of BIH as electron source (bar columns represent average product formation in μmol and error bar corresponds to standard deviation determined from 3 set of experimental data. Scatters represent TON).

calculated with the addition of a Ru(tpy)(bpy) unit terminating at 31% open pore volume for a simulation cell with one unit loading on each node.

The optimized structures with different bpy and Ru loadings were then used to calculate the surface area using the Monte Carlo Widom N_2 insertion technique. We find an exceptional agreement between experimental (1874 m^2/g) and calculated (1754 m^2/g) surface areas (see Figure 3b) for MOF-808, while for bpy@MOF-808, the experimental and calculated values for the 2bpy/node loading are 1228 m^2/g and 1247 m^2/g, respectively. We also ran molecular dynamics simulations for Ru@MOF-808 at varying loadings of Ru-complex. We find that the amount of Ru-complex loading is greatly affected by the sterics and that the loadings of more than one Ru cluster per node lead to almost complete loss of accessible surface area (Figure 3b). The calculated surface area as a function of Ru-loading shows that the loading of 0.6 Ru clusters resulted in a surface area value that is in good agreement with the observed experimental value (1233 vs 1323 m^2/g). Overall, our combined experimental and computational work indicates successful postsynthetic modification of MOF-808 at the loading of 2bpy/node for bpy@MOF-808 and 0.6Ru/node for Ru@MOF-808.

3.2. Photochemical CO_2 Reduction by Ru@MOF-808. The photocatalytic CO_2 reduction by Ru@MOF-808 was evaluated under several different experimental conditions (Figure 5a and Supporting Information) and CO and $HCOO^-$ were identified as products in all cases. MOF-808, under photochemical conditions, failed to perform CO_2 reduction, pointing to $Ru(tpy)(bpy)ACN^{2+}$ as the source for the observed activity (Figure S7). Although the lowest energy excited-state of $Ru(tpy)(bpy)^{2+}$ is short-lived (470 ps), excess amount of sacrificial agent, BIH, facilitates rapid quenching of the excited state in the reaction.[50] Among the sacrificial electron donors tested (TEOA, BNAH, BIH), BIH was found to be crucial in initiating the catalytic cycle, likely by reductive quenching the excited state of the Ru-complex ($Ru^{(2+*/1+)}$ = 1.01 V vs NHE).[51] This result is consistent with the fact that BIH is the strongest reductant ($E_{1/2}^0$ ($BIH^{\bullet+}$/BIH) = 0.56 V; $E_{1/2}^0$ ($BNAH^{\bullet+}$/BNAH) = 0.89 V; $E_{1/2}^0$ ($TEOA^{\bullet+}$/TEOA) = 1.07 V).[52,53] In addition, a Stern−Volmer quenching constant of K_{SV} = 1.83 × 10^3 M^{-1} was determined from phosphorescence emission spectra of $Ru(tpy)(bpy)ACN^{2+}$ in the presence of BIH as quencher (Figure S9). The addition of TEOA along with BIH resulted in an increase of the formate yield, while little variation was found in CO production as shown in Figure 5a. This finding is consistent with a previous report by Fujita and coauthors, who showed that TEOA captures CO_2 into a zwitterionic alkyl carbonate adduct and has a vital role in the catalytic generation of formate by enhancing the hydride transfer kinetics by several orders of magnitude.[25] However, TEOA has a negative effect on our framework and has led to the gradual disintegration of Ru@MOF-808.

It is interesting that, even in the absence of TEOA, some amount of formate was observed, indicating the possible role of Ru@MOF-808 in exhibiting similar CO_2 capture and hydride transfer kinetics enhancements as TEOA. To evaluate this effect, we performed comparative photocatalytic experiments for Ru@MOF-808 and the corresponding model compound in the absence of framework, Rutpybpy-ACN, by ensuring an equal amount of Ru sites in both cases. These experiments were conducted in CO_2-saturated ACN/H_2O solvent mixture in the presence of BIH as the electron donor. Interestingly, this study revealed that Rutpybpy-ACN generates more CO, whereas Ru@MOF-808 outperformed the former in formate production, as shown in Figure 5b,c. Control experiments were conducted to reveal the role of each component involved in photocatalysis (Supporting Information, Table S3, entries 8 and 10−12). Neither CO nor formate was detected in the absence of light and Ru@MOF-808 indicating the process is purely photon-mediated and that Ru centers are essential for catalysis. In the absence of water, the formation of reduced products is heavily suppressed, suggesting that water might be acting as a proton relay or proton source. Similar effects of water on catalytic CO_2 reduction have been reported previously.[54,55] The photoirradiated mixture in the absence of CO_2 was incapable of producing CO and formate, justifying the origin of obtained reduced chemicals is from the supplied CO_2. In addition, the structural integrity of Ru@MOF-808 after photocatalysis was found to be preserved with a minimal extent of damage, as indicated by pXRD pattern (Figure S8).

https://doi.org/10.1021/acs.inorgchem.5c02600
Inorg. Chem. 2025, 64, 18304−18315

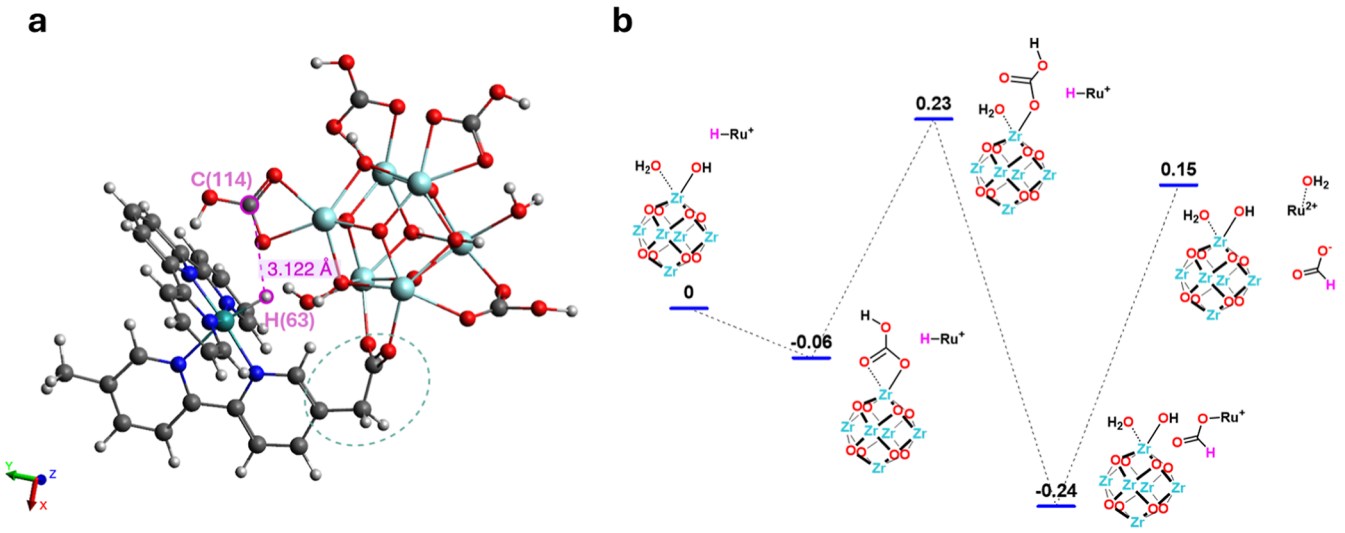

Figure 6. (a) Optimized structure of bicarbonate-bound Ru−H@MOF-808 showing the proximal distance between the H atom of Ru−H(63) and the carbon atom of C(114)(O)(OH)O−Zr. The dotted ellipsoid indicates the Ru−H unit is anchored on the same Zr-oxo node where Zr-bicarbonate is generated. (b) Free energy profile in eV, computed using ORCA 6.0 for the conversion of captured CO_2 into formate.

The recyclability test was performed on the Ru@MOF-808 catalyst to investigate its stability (Figure S10). A severe loss of activity toward CO and $HCOO^-$ formation is observed after the first cycle, which may be a direct consequence of leaching of Ru-sites from the Zr-nodes, catalyst fouling, and/or clogging of MOF pores. To assess whether formate poisoning is responsible for catalyst inactivation, we compared product yields from cycling experiments using MOF samples that were either used as recovered from the prior cycle or thermally activated to remove the bound formate ligand (Figure S12). The resulting formate and CO yields do not change significantly across two sets of samples, indicating that formate poisoning is not the leading cause of catalyst deactivation. Loss of Ru-sites from the Zr-nodes has been confirmed from the difference absorption spectra of reaction supernatants before and after the first cycle of photoirradiation, as shown in Figure S11. This finding supports the leaching of Ru-sites from the MOF as the main cause for the loss of catalytic activity.

In any case, the difference observed in the CO/formate ratios between Ru@MOF-808 and Rutpybpy-ACN suggests that the framework somehow facilitates the formate formation.[56−59] This finding is particularly interesting in light of our recent findings that the Zr-nodes play an important role in capturing CO_2 in the form of Zr-bicarbonate species, which are photochemically reduced to formate in the presence of appropriate sacrificial donors.[60] The formation of CO likely follows a mechanism involving a Ru−COOH intermediate (Supporting Information, Scheme S1) as proposed previously for similar catalysts.[30,40] Here, we focus on the increased formate selectivity and hypothesize a cooperative mechanism involving CO_2 capture by Zr-based nodes and a subsequent hydride transfer from photochemically generated Ru-hydride to the neighboring Zr-bicarbonate of the node. The photochemical formation of Ru-hydride has been previously reported in studies involving the molecular $Ru(tpy)(bpy)^{2+}$ complex,[39] and we hypothesize that a similar process occurs in the MOF-bound Ru complex. To assess the feasibility of hydride transfer from Ru-hydride to Zr-bicarbonate, we conducted two sets of DFT calculations. First, we performed a conformational search to identify spatial arrangements that allow close interactions between the node-bound Ru-hydride and node-bound bicarbonate (Figure 6a). This analysis determines whether structural constraints permit sufficient proximity between the hydride donor and acceptor moieties. Second, we evaluated the thermodynamics of a plausible hydride transfer mechanism, which involves: (i) CO_2 reaction with Zr−OH groups at the node; (ii) activation of Zr-bicarbonate via water coordination; (iii) hydride transfer from Ru−H to Zr-bicarbonate, and (iv) formate ion release (Figure 6b).

To provide insights into increased formate selectivity by Ru@MOF-808, a computational search for close contact between photogenerated Ru(tpy)(bpy)-hydride and Zr-bicarbonate moieties was performed (Section S4.2). The node-anchored Ru-complex is relatively rigid and can change its orientation only through the rotation of two C−C bonds of the bpy-COOH moiety of Ru@MOF-808. Thus, we rotated the two neighboring single C−C bonds at the one-degree sampling resolution, yielding a total of 129,600 conformations. Then, we evaluated the close-contact conformations in which the Ru−H group is within several Angstroms from the node-bound CO_2 in the form of a Zr-bicarbonate. This computational analysis revealed three close contact conformations, two of which involve interactions across two different Zr-nodes, one containing Ru-complex and another containing Zr-bicarbonate, as shown in Figure S12. One of the structures involves a single node that contains both the Ru-hydride and the Zr-bicarbonate moiety, as shown Figure 6A. This structure is particularly appealing, as it resembles the commonly observed four-membered transition-state structure for CO_2 insertion into metal-H bonds.[61] The structure shown in Figure 6A exhibits an interatomic H···C distance of only 3.1 Å (H from Ru−H and C from Zr-bicarbonate). Such a proximal distance could enable the hydride to react with the captured CO_2 and produce a Ru-formato complex (Ru−OCHO@MOF-808) within the MOF framework.

Given that the hydride-bicarbonate close contacts have been identified through the conformational search, we further evaluated the Gibbs free energies for the key steps of the proposed reduction mechanism (Figure 6b). To simplify the

https://doi.org/10.1021/acs.inorgchem.5c02600
Inorg. Chem. 2025, 64, 18304−18315

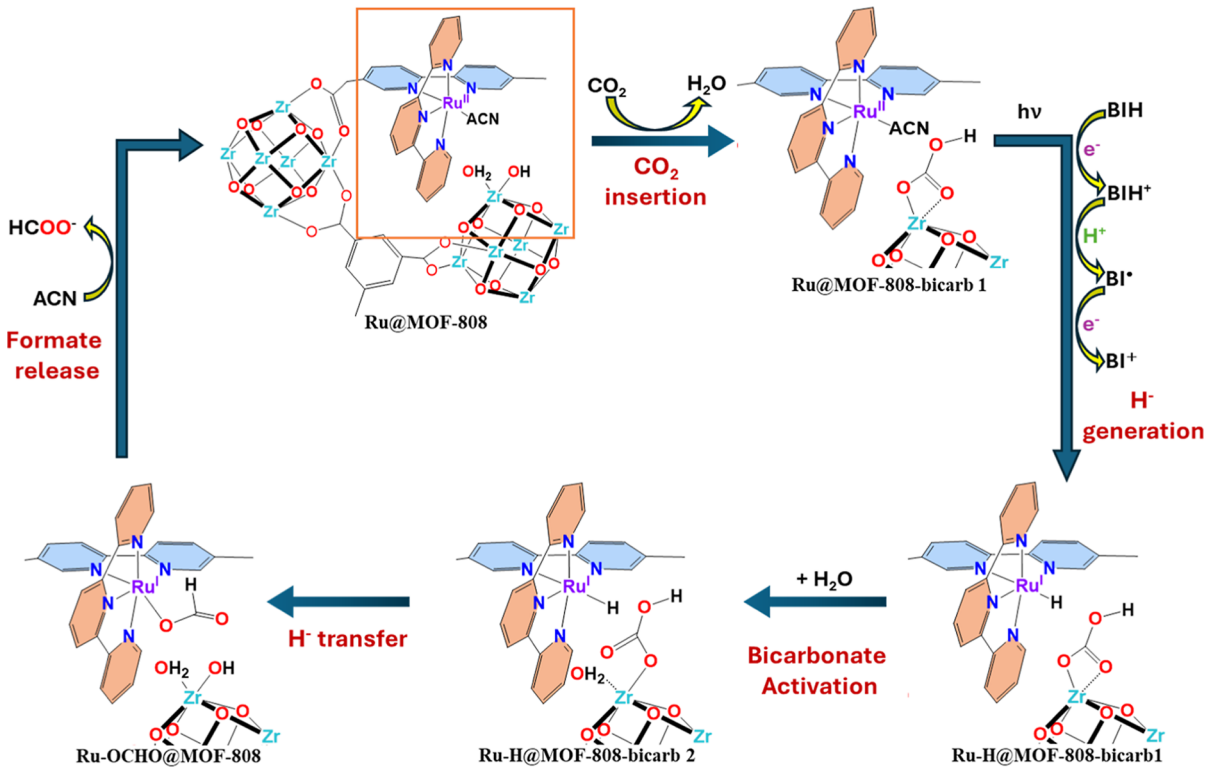

Figure 7. Proposed mechanism of photocatalytic $HCOO^-$ formation by Ru@MOF-808. For clarity, the square boxed part in the top left corner structure is used to depict the possible intermediates.

calculation cost, these experiments were performed using Ru−H that is not bound to the Zr node. The bidentate bicarbonate geometry was chosen based on previous computational findings showing that bidentate bicarbonate exhibits lower Gibbs free energy than the bridging bicarbonate motif.[60] The addition of CO_2 into the Zr−OH bond to form a bidentate bicarbonate species was found to be thermodynamically favorable with Gibs free energy of −0.06 eV. Similar CO_2 insertion reactivity has been reported with Ni and Zn complexes where the kinetics of the insertion reaction is shown to be dependent on the nucleophilicity of the functional group involved.[62−65] Interestingly, our previous study involving CO_2 insertion into the Zr−OH bond of a different MOF yielded a Gibbs free energy of G = +0.18 eV.[60] The differences in calculated energies may be associated with different computational methods used in the two studies or with the small differences in the node structures of the two MOFs. Each node of Ru@MOF-808 features five Zr−OH groups capable of inserting CO_2 to form Zr-bicarbonate adducts, offering abundant sites for substrate binding near the metal catalyst. The second step of the proposed reduction involves the activation of Zr-bound bicarbonate through water coordination and the formation of the monodentate adduct. This structural change is energetically uphill with ΔG = +0.29 eV, as shown in Figure 6b. While not spontaneous under standard conditions, this reaction is likely spontaneous under our reaction conditions, where excess water is present in the solution. The third step of the proposed catalytic cycle involves the transfer of hydride ion. The product of direct hydride transfer step is a tetrahedral Ru−Zr adduct intermediate shown in Figure S14. However, we postulate that this intermediate is not likely to be formed, given the high energy penalty associated with its formation (ΔG = +0.70 eV). Instead, we propose that the hydride transfer proceeds in concert with the cleavage of C−O bond to form Ru-formato complex and the recovery of the Zr-hydroxo-aqua node. This step is calculated to be a thermodynamically favorable product by ΔG = −0.471 eV. The final step of the proposed reduction involves the dissociation of the Ru-formato complex to release the formate ion. We find this step to be uphill by 0.39 eV, which is consistent with the results shown by Fujita et al. on a similar Ru-polypyridyl complex.[25]

Overall, our experimental and computational analyses indicate that the increased formate production may follow a mechanism illustrated in Figure 7, which starts with the capture of carbon dioxide by the MOF node to form the Zr-bicarbonate intermediate Ru@MOF-808-bicarb1. The proposed photochemical step involves reductive quenching of the photoexcited Rutpybpy unit in Ru@MOF-808 using BIH as the sacrificial donor to form the Ru-hydride intermediate Ru−H@MOF-808-bicarb1. While this process involves an overall transfer of the hydride ion, it likely occurs via a sequence of electron and proton transfer steps, as was previously shown for the molecular analog.[39] Further activation of zirconium-bound bidentate bicarbonate into monodentate bicarbonate Ru−H@MOF-808-bicarb2, followed by transfer of hydride to form Ru−OCHO@MOF-808 is proposed. The catalytic cycle is finally closed with the release of formate ion and regeneration of Ru@MOF-808. This mechanism illustrates the ability of Zr-based MOFs to host the catalytic sites, as well as to immobilize CO_2 and promote target transformations.

4. CONCLUSION

In summary, we report the photocatalytic CO_2 reduction by Ru@MOF-808, a porous Zr-based MOF that has been postsynthetically modified with a well-known Ru-based

https://doi.org/10.1021/acs.inorgchem.5c02600
Inorg. Chem. 2025, 64, 18304−18315

catalyst, $Ru(tpy)(bpy)^{2+}$. Our extensive experimental characterization of Ru@MOF-808, supported by theoretical calculations, revealed that the Ru-moieties are incorporated at a loading of almost one Ru per Zr node. The photochemical CO_2 reduction was evaluated in the presence of several sacrificial electron donors, and we found that only BIH is sufficiently reducing to enable the reductive quenching of the Ru-based excited state. The CO_2 was reduced to C1 products CO and formate. Interestingly, the formate yield was found to increase in Ru-modified MOF catalyst relative to the performance of the homogeneous Ru-based model analog, indicating that the MOF scaffold increases the formate selectivity. Based on our results and previous literature reports, we propose a mechanism that involves the capture of CO_2 in the form of node-bound Zr-bicarbonate, which is reduced via hydride transfer from the photogenerated Ru−H intermediate. While formate is a minor product in this reaction, we anticipate that the formate selectivity can be further increased by a further optimization of relative geometry of metal hydride complex relative to the Zr-bound bicarbonate. This study demonstrates that the Zr-based MOF nodes provide an ideal platform that not only accommodates photocatalytic units, but also captures CO_2, enabling photoreactive CO_2 capture processes.

■ ASSOCIATED CONTENT

Supporting Information

The Supporting Information is available free of charge at https://pubs.acs.org/doi/10.1021/acs.inorgchem.5c02600.

Document briefs on the synthetic procedures, details of characterizations and photochemical CO_2RR experiments and computational details. The structures used for various calculations are also included (PDF)

■ AUTHOR INFORMATION

Corresponding Author

Ksenija D. Glusac − *Department of Chemistry, University of Illinois Chicago, Chicago, Illinois 60607, United States; Chemical Sciences and Engineering, Argonne National Laboratory, Lemont, Illinois 60439, United States;* orcid.org/0000-0002-2734-057X; Email: glusac@uic.edu

Authors

Rosmi Reji − *Department of Chemistry, University of Illinois Chicago, Chicago, Illinois 60607, United States; Chemical Sciences and Engineering, Argonne National Laboratory, Lemont, Illinois 60439, United States*

Juan P. Vizuet − *Department of Chemistry, University of Illinois Chicago, Chicago, Illinois 60607, United States;* orcid.org/0000-0002-3660-2041

Xiaoli Yan − *Department of Civil, Materials, and Environmental Engineering, University of Illinois Chicago, Chicago, Illinois 60607, United States; Data Science and Learning Division, Argonne National Laboratory, Lemont, Illinois 60439, United States;* orcid.org/0000-0002-6512-2338

Biki K. Behera − *Department of Chemistry, University of Illinois Chicago, Chicago, Illinois 60607, United States*

Xin Zheng − *Department of Chemistry, University of Illinois Chicago, Chicago, Illinois 60607, United States;* orcid.org/0000-0002-5506-8112

Matthew Klenk − *Materials Science Division, Argonne National Laboratory, Lemont, Illinois 60439, United States*

Nicholas P. Weingartz − *Department of Chemistry, Northwestern University, Evanston, Illinois 60201, United States*

George T. Kostopoulos − *Department of Chemistry, University of Illinois Chicago, Chicago, Illinois 60607, United States*

Lin X. Chen − *Chemical Sciences and Engineering, Argonne National Laboratory, Lemont, Illinois 60439, United States; Department of Chemistry, Northwestern University, Evanston, Illinois 60201, United States;* orcid.org/0000-0002-8450-6687

Peter Zapol − *Materials Science Division, Argonne National Laboratory, Lemont, Illinois 60439, United States;* orcid.org/0000-0003-0570-9169

Neeraj Agarwal − *UM-DAE Centre for Excellence in Basic Sciences, University of Mumbai, Mumbai 400098, India;* orcid.org/0000-0003-2853-2730

Eliu Huerta − *Data Science and Learning Division, Argonne National Laboratory, Lemont, Illinois 60439, United States; Department of Computer Science, The University of Chicago, Chicago, Illinois 60637, United States*

Murat Keceli − *Computational Science Division, Argonne National Laboratory, Lemont, Illinois 60439, United States;* orcid.org/0000-0001-8588-9272

Santanu Chaudhuri − *Chemical Sciences and Engineering, Argonne National Laboratory, Lemont, Illinois 60439, United States;* orcid.org/0000-0002-4328-2947

Complete contact information is available at: https://pubs.acs.org/10.1021/acs.inorgchem.5c02600

Author Contributions

R.R. designed and performed the experimental work, processed and analyzed experimental data and wrote the manuscript. J.P.V., B.K.B., X.Z. and G.T.K. helped in the synthesis and/or characterization of the materials used. Matthew Klenk and P.Z. performed all periodic DFT calculations and MOF surface area evaluations. N.P.W. and L.X.C. helped with the collection and analysis of XAFS data. X.Yan, E.H., and Murat Keceli provided computational support by performing DFT calculations on the proposed reaction mechanism. K.D.G. conceived the project, contributed to data analysis and interpretation, and played a supporting role in writing the manuscript.

Notes

The authors declare no competing financial interest.

■ ACKNOWLEDGMENTS

This work is supported by the U.S. Department of Energy (DOE), Office of Science, Office of Basic Energy Science, Division of Chemical Sciences, Geosciences, and Biosciences through Argonne National Laboratory under Contract No. DE-AC02-06CH11357. We thank Mahsa Zarifi for assisting in collecting and summarizing the literature on photophysical and photochemical studies of Ru complexes. Matthew Klenk and P.Z. gratefully acknowledge the computing resources provided by the Laboratory Computing Resource Center at Argonne National Laboratory. This research used resources of the Argonne Leadership Computing Facility, a U.S. Department of Energy (DOE) Office of Science user facility at Argonne National Laboratory and is based on research supported by the U.S. DOE Office of Science-Advanced Scientific Computing

Research Program, under Contract No. DE-AC02-06CH11357.

REFERENCES

(1) Aresta, M.; Dibenedetto, A.; Angelini, A. Catalysis for the Valorization of Exhaust Carbon: From CO_2 to Chemicals, Materials, and Fuels. Technological Use of CO_2. *Chem. Rev.* **2014**, *114* (3), 1709−1742.

(2) Yoshino, S.; Iwase, A.; Yamaguchi, Y.; Suzuki, T. M.; Morikawa, T.; Kudo, A. Photocatalytic CO_2 Reduction Using Water as an Electron Donor under Visible Light Irradiation by Z-Scheme and Photoelectrochemical Systems over $(CuGa)_{0.5}ZnS_2$ in the Presence of Basic Additives. *J. Am. Chem. Soc.* **2022**, *144* (5), 2323−2332.

(3) Goeppert, A.; Czaun, M.; Jones, J.-P.; Surya Prakash, G. K.; Olah, G. A. Recycling of Carbon Dioxide to Methanol and Derived Products − Closing the Loop. *Chem. Soc. Rev.* **2014**, *43* (23), 7995−8048.

(4) Sun, K.; Qian, Y.; Jiang, H. Metal-Organic Frameworks for Photocatalytic Water Splitting and CO_2 Reduction. *Angew. Chem., Int. Ed.* **2023**, *62* (15), No. e202217565.

(5) Karmakar, S.; Barman, S.; Rahimi, F. A.; Rambabu, D.; Nath, S.; Maji, T. K. Confining Charge-Transfer Complex in a Metal-Organic Framework for Photocatalytic CO_2 Reduction in Water. *Nat. Commun.* **2023**, *14* (1), 4508.

(6) Li, J.; Huang, H.; Xue, W.; Sun, K.; Song, X.; Wu, C.; Nie, L.; Li, Y.; Liu, C.; Pan, Y.; Jiang, H.-L.; Mei, D.; Zhong, C. Self-Adaptive Dual-Metal-Site Pairs in Metal-Organic Frameworks for Selective CO_2 Photoreduction to CH_4. *Nat. Catal.* **2021**, *4* (8), 719−729.

(7) Karmakar, S.; Barman, S.; Rahimi, F. A.; Maji, T. K. Covalent Grafting of Molecular Photosensitizer and Catalyst on MOF-808: Effect of Pore Confinement toward Visible Light-Driven CO_2 Reduction in Water. *Energy Environ. Sci.* **2021**, *14* (4), 2429−2440.

(8) Karmakar, S.; Barman, S.; Rahimi, F. A.; Biswas, S.; Nath, S.; Maji, T. K. Developing Post-Modified Ce-MOF as a Photocatalyst: A Detail Mechanistic Insight into CO_2 Reduction toward Selective C2 Product Formation. *Energy Environ. Sci.* **2023**, *16* (5), 2187−2198.

(9) Zhuo, T.-C.; Song, Y.; Zhuang, G.-L.; Chang, L.-P.; Yao, S.; Zhang, W.; Wang, Y.; Wang, P.; Lin, W.; Lu, T.-B.; Zhang, Z.-M. H-Bond-Mediated Selectivity Control of Formate versus CO during CO_2 Photoreduction with Two Cooperative Cu/X Sites. *J. Am. Chem. Soc.* **2021**, *143* (16), 6114−6122.

(10) Feng, X.; Pi, Y.; Song, Y.; Brzezinski, C.; Xu, Z.; Li, Z.; Lin, W. Metal−Organic Frameworks Significantly Enhance Photocatalytic Hydrogen Evolution and CO_2 Reduction with Earth-Abundant Copper Photosensitizers. *J. Am. Chem. Soc.* **2020**, *142* (2), 690−695.

(11) Stanley, P. M.; Thomas, C.; Thyrhaug, E.; Urstoeger, A.; Schuster, M.; Hauer, J.; Rieger, B.; Warnan, J.; Fischer, R. A. Entrapped Molecular Photocatalyst and Photosensitizer in Metal−Organic Framework Nanoreactors for Enhanced Solar CO_2 Reduction. *ACS Catal.* **2021**, *11* (2), 871−882.

(12) Huang, N.-Y.; He, H.; Liu, S.; Zhu, H.-L.; Li, Y.-J.; Xu, J.; Huang, J.-R.; Wang, X.; Liao, P.-Q.; Chen, X.-M. Electrostatic Attraction-Driven Assembly of a Metal−Organic Framework with a Photosensitizer Boosts Photocatalytic CO_2 Reduction to CO. *J. Am. Chem. Soc.* **2021**, *143* (42), 17424−17430.

(13) Wang, C.; Xie, Z.; DeKrafft, K. E.; Lin, W. Doping Metal−Organic Frameworks for Water Oxidation, Carbon Dioxide Reduction, and Organic Photocatalysis. *J. Am. Chem. Soc.* **2011**, *133* (34), 13445−13454.

(14) Fei, H.; Sampson, M. D.; Lee, Y.; Kubiak, C. P.; Cohen, S. M. Photocatalytic CO_2 Reduction to Formate Using a Mn(I) Molecular Catalyst in a Robust Metal−Organic Framework. *Inorg. Chem.* **2015**, *54* (14), 6821−6828.

(15) Canivet, J.; Wisser, F. M. Metal−Organic Framework Catalysts for Solar Fuels: Light-Driven Conversion of Carbon Dioxide into Formic Acid. *ACS Appl. Energy Mater.* **2023**, *6* (18), 9027−9043.

(16) Wang, X.; Wisser, F. M.; Canivet, J.; Fontecave, M.; Mellot-Draznieks, C. Immobilization of a Full Photosystem in the Large-Pore MIL-101 Metal−Organic Framework for CO_2 Reduction. *ChemSusChem* **2018**, *11* (18), 3315−3322.

(17) Stanley, P. M.; Haimerl, J.; Thomas, C.; Urstoeger, A.; Schuster, M.; Shustova, N. B.; Casini, A.; Rieger, B.; Warnan, J.; Fischer, R. A. Host−Guest Interactions in a Metal−Organic Framework Isoreticular Series for Molecular Photocatalytic CO_2 Reduction. *Angew. Chem., Int. Ed.* **2021**, *60* (33), 17854−17860.

(18) Zhang, K.; Goswami, S.; Noh, H.; Lu, Z.; Sheridan, T.; Duan, J.; Dong, W.; Hupp, J. T. An Iron-Porphyrin Grafted Metal−Organic Framework as a Heterogeneous Catalyst for the Photochemical Reduction of CO_2. *J. Photochem. Photobiol.* **2022**, *10*, 100111.

(19) Yang, Y.; Zhang, H.; Wang, Y.; Shao, L.; Fang, L.; Dong, H.; Lu, M.; Dong, L.; Lan, Y.; Zhang, F. Integrating Enrichment, Reduction, and Oxidation Sites in One System for Artificial Photosynthetic Diluted CO_2 Reduction. *Adv. Mater.* **2023**, *35* (40), 2304170.

(20) Elgrishi, N.; Chambers, M. B.; Wang, X.; Fontecave, M. Molecular Polypyridine-Based Metal Complexes as Catalysts for the Reduction of CO_2. *Chem. Soc. Rev.* **2017**, *46* (3), 761−796.

(21) Chen, Z.; Chen, C.; Weinberg, D. R.; Kang, P.; Concepcion, J. J.; Harrison, D. P.; Brookhart, M. S.; Meyer, T. J. Electrocatalytic Reduction of CO_2 to CO by Polypyridyl Ruthenium Complexes. *Chem. Commun.* **2011**, *47* (47), 12607.

(22) Assaf, E. A.; Gonell, S.; Chen, C.-H.; Miller, A. J. M. Accessing and Photo-Accelerating Low-Overpotential Pathways for CO_2 Reduction: A Bis-Carbene Ruthenium Terpyridine Catalyst. *ACS Catal.* **2022**, *12* (20), 12596−12606.

(23) Johnson, B. A.; Agarwala, H.; White, T. A.; Mijangos, E.; Maji, S.; Ott, S. Judicious Ligand Design in Ruthenium Polypyridyl CO_2 Reduction Catalysts to Enhance Reactivity by Steric and Electronic Effects. *Chem.—Eur. J.* **2016**, *22* (42), 14870−14880.

(24) Johnson, B. A.; Maji, S.; Agarwala, H.; White, T. A.; Mijangos, E.; Ott, S. Activating a Low Overpotential CO_2 Reduction Mechanism by a Strategic Ligand Modification on a Ruthenium Polypyridyl Catalyst. *Angew. Chem., Int. Ed.* **2016**, *55* (5), 1825−1829.

(25) Sampaio, R. N.; Grills, D. C.; Polyansky, D. E.; Szalda, D. J.; Fujita, E. Unexpected Roles of Triethanolamine in the Photochemical Reduction of CO_2 to Formate by Ruthenium Complexes. *J. Am. Chem. Soc.* **2020**, *142* (5), 2413−2428.

(26) Ishida, H.; Tanaka, H.; Tanaka, K.; Tanaka, T. Selective Formation of HCOO − in the Electrochemical CO_2 Reduction Catalysed by $[Ru(Bpy)_2(CO)_2]^{2+}$ (Bpy = 2,2′-Bipyridine). *J. Chem. Soc., Chem. Commun.* **1987**, No. 2, 131−132.

(27) Ishida, H.; Tanaka, K.; Tanaka, T. Electrochemical CO_2 Reduction Catalyzed by Ruthenium Complexes $[Ru(Bpy)_2(CO)_2]^{2+}$ and $[Ru(Bpy)_2(CO)Cl]^+$. Effect of PH on the Formation of CO and $HCOO^-$. *Organometallics* **1987**, *6* (1), 181−186.

(28) Agarwala, H.; Chen, X.; Lyonnet, J. R.; Johnson, B. A.; Ahlquist, M.; Ott, S. Alternating Metal-Ligand Coordination Improves Electrocatalytic CO_2 Reduction by a Mononuclear Ru Catalyst. *Angew. Chem.* **2023**, *135* (17), No. e202218728.

(29) Chen, Z.; Chen, C.; Weinberg, D. R.; Kang, P.; Concepcion, J. J.; Harrison, D. P.; Brookhart, M. S.; Meyer, T. J. Electrocatalytic Reduction of CO_2 to CO by Polypyridyl Ruthenium Complexes. *Chem. Commun.* **2011**, *47*, 12607−12609.

(30) Schneider, T. W.; Hren, M. T.; Ertem, M. Z.; Angeles-Boza, A. M. [Ru II (Tpy)(Bpy)Cl]$^+$-Catalyzed Reduction of Carbon Dioxide. Mechanistic Insights by Carbon-13 Kinetic Isotope Effects. *Chem. Commun.* **2018**, *54* (61), 8518−8521.

(31) Kern, S.; van Eldik, R. Mechanistic Insight from Activation Parameters for the Reaction of a Ruthenium Hydride Complex with CO_2 in Conventional Solvents and an Ionic Liquid. *Inorg. Chem.* **2012**, *51* (13), 7340−7345.

(32) Pugh, J. R.; Bruce, M. R. M.; Sullivan, B. P.; Meyer, T. J. Formation of a Metal-Hydride Bond and the Insertion of Carbon Dioxide. Key Steps in the Electrocatalytic Reduction of Carbon Dioxide to Formate Anion. *Inorg. Chem.* **1991**, *30* (1), 86−91.

https://doi.org/10.1021/acs.inorgchem.5c02600
Inorg. Chem. 2025, 64, 18304−18315

(33) Matsubara, Y.; Fujita, E.; Doherty, M. D.; Muckerman, J. T.; Creutz, C. Thermodynamic and Kinetic Hydricity of Ruthenium(II) Hydride Complexes. *J. Am. Chem. Soc.* **2012**, *134* (38), 15743−15757.
(34) Konno, H.; Kobayashi, A.; Sakamoto, K.; Fagalde, F.; Katz, N. E.; Saitoh, H.; Ishitani, O. Synthesis and Properties of $[Ru(Tpy)(4,4'-X_2bpy)H]^+$ (Tpy = 2,2′:6′,2″-Terpyridine, Bpy = 2,2′-Bipyridine, X = H and MeO), and Their Reactions with CO_2. *Inorg. Chim. Acta* **2000**, *299* (2), 155−163.
(35) Nagao, H.; Mizukawa, T.; Tanaka, K. Carbon-Carbon Bond Formation in the Electrochemical Reduction of Carbon Dioxide Catalyzed by a Ruthenium Complex. *Inorg. Chem.* **1994**, *33* (15), 3415−3420.
(36) Müller, A. V.; Ahmad, S.; Sirlin, J. T.; Ertem, M. Z.; Polyansky, D. E.; Grills, D. C.; Meyer, G. J.; Sampaio, R. N.; Concepcion, J. J. Reduction of CO to Methanol with Recyclable Organic Hydrides. *J. Am. Chem. Soc.* **2024**, *146* (15), 10524−10536.
(37) Jakubikova, E.; Chen, W.; Dattelbaum, D. M.; Rein, F. N.; Rocha, R. C.; Martin, R. L.; Batista, E. R. Electronic Structure and Spectroscopy of $[Ru(Tpy)_2]^{2+}$, $[Ru(Tpy)(Bpy)(H_2O)]^{2+}$, and $[Ru(Tpy)(Bpy)(Cl)]^+$. *Inorg. Chem.* **2009**, *48* (22), 10720−10725.
(38) Siewert, B.; Langerman, M.; Hontani, Y.; Kennis, J. T. M.; van Rixel, V. H. S.; Limburg, B.; Siegler, M. A.; Talens Saez, V.; Kieltyka, R. E.; Bonnet, S. Turning on the Red Phosphorescence of a [Ru(Tpy)(Bpy)(Cl)]Cl Complex by Amide Substitution: Self-Aggregation, Toxicity, and Cellular Localization of an Emissive Ruthenium-Based Amphiphile. *Chem. Commun.* **2017**, *53* (81), 11126−11129.
(39) Matsubara, Y.; Konno, H.; Kobayashi, A.; Ishitani, O. Quantitative Photochemical Formation of $[Ru(Tpy)(Bpy)H]^+$. *Inorg. Chem.* **2009**, *48* (21), 10138−10145.
(40) Lee, S. K.; Kondo, M.; Okamura, M.; Enomoto, T.; Nakamura, G.; Masaoka, S. Function-Integrated Ru Catalyst for Photochemical CO_2 Reduction. *J. Am. Chem. Soc.* **2018**, *140* (49), 16899−16903.
(41) Queyriaux, N.; Swords, W. B.; Agarwala, H.; Johnson, B. A.; Ott, S.; Hammarström, L. Mechanistic Insights on the Non-Innocent Role of Electron Donors: Reversible Photocapture of CO_2 by Ru^{II}-Polypyridyl Complexes. *Dalton Trans.* **2019**, *48* (45), 16894−16898.
(42) Reji, R.; Vizuet, J. P.; Yan, X.; Behera, B.; Zheng, X.; Klenk, M.; Weingartz, N. P.; Kostopoulos, G. T.; Chen, L. X.; Agarwal, N.; Zapol, P.; Huerta, E. A.; Keceli, M.; Glusac, K. Product Selectivity in Photochemical CO_2 Reduction by a Post-Synthetically Modified Zr-MOF. *ChemRxiv* **2025**, chemrxiv-2025-jjcbv.
(43) Aunan, E.; Affolter, C. W.; Olsbye, U.; Lillerud, K. P. Modulation of the Thermochemical Stability and Adsorptive Properties of MOF-808 by the Selection of Non-Structural Ligands. *Chem. Mater.* **2021**, *33* (4), 1471−1476.
(44) Deria, P.; Mondloch, J. E.; Tylianakis, E.; Ghosh, P.; Bury, W.; Snurr, R. Q.; Hupp, J. T.; Farha, O. K. Perfluoroalkane Functionalization of NU-1000 via Solvent-Assisted Ligand Incorporation: Synthesis and CO_2 Adsorption Studies. *J. Am. Chem. Soc.* **2013**, *135* (45), 16801−16804.
(45) Romero-Muñiz, I.; Romero-Muñiz, C.; del Castillo-Velilla, I.; Marini, C.; Calero, S.; Zamora, F.; Platero-Prats, A. E. Revisiting Vibrational Spectroscopy to Tackle the Chemistry of Zr_6O_8 Metal-Organic Framework Nodes. *ACS Appl. Mater. Interfaces* **2022**, *14* (23), 27040−27047.
(46) Yi, K.; Li, H.; Zhang, X.; Zhang, L. Designed Tb(III)-Functionalized MOF-808 as Visible Fluorescent Probes for Monitoring Bilirubin and Identifying Fingerprints. *Inorg. Chem.* **2021**, *60* (5), 3172−3180.
(47) Liu, J.; Frenkel, A. I. Multiple-Scattering EXAFS Analysis. In *International Tables for Crystallography*; Wiley, 2022; pp 645−652.
(48) Co, M. S.; Hendrickson, W. A.; Hodgson, K. O.; Doniach, S. Multiple-Scattering Effects in EXAFS Spectroscopy of Oxygen-Bridged Iron Complexes. Possibility of Angle Determination of EXAFS Analysis. *J. Am. Chem. Soc.* **1983**, *105* (5), 1144−1150.
(49) Silvestre-Albero, A. M.; Juárez-Galán, J. M.; Silvestre-Albero, J.; Rodríguez-Reinoso, F. Low-Pressure Hysteresis in Adsorption: An Artifact? *J. Phys. Chem. C* **2012**, *116* (31), 16652−16655.
(50) Knoll, J. D.; Albani, B. A.; Turro, C. Excited State Investigation of a New Ru(ii) Complex for Dual Reactivity with Low Energy Light. *Chem. Commun.* **2015**, *51* (42), 8777−8780.
(51) Bock, C. R.; Connor, J. A.; Gutierrez, A. R.; Meyer, T. J.; Whitten, D. G.; Sullivan, B. P.; Nagle, J. K. Estimation of Excited-State Redox Potentials by Electron-Transfer Quenching. Application of Electron-Transfer Theory to Excited-State Redox Processes. *J. Am. Chem. Soc.* **1979**, *101* (17), 4815−4824.
(52) Zhu, X.-Q.; Zhang, M.-T.; Yu, A.; Wang, C.-H.; Cheng, J.-P. Hydride, Hydrogen Atom, Proton, and Electron Transfer Driving Forces of Various Five-Membered Heterocyclic Organic Hydrides and Their Reaction Intermediates in Acetonitrile. *J. Am. Chem. Soc.* **2008**, *130* (8), 2501−2516.
(53) Manke, A.-M.; Geisel, K.; Fetzer, A.; Kurz, P. A Water-Soluble Tin(iv) Porphyrin as a Bioinspired Photosensitiser for Light-Driven Proton-Reduction. *Phys. Chem. Chem. Phys.* **2014**, *16* (24), 12029−12042.
(54) Lim, C.-H.; Holder, A. M.; Musgrave, C. B. Mechanism of Homogeneous Reduction of CO_2 by Pyridine: Proton Relay in Aqueous Solvent and Aromatic Stabilization. *J. Am. Chem. Soc.* **2013**, *135* (1), 142−154.
(55) Wang, Y.; Liu, T.; Chen, L.; Chao, D. Water-Assisted Highly Efficient Photocatalytic Reduction of CO_2 to CO with Noble Metal-Free Bis(Terpyridine)Iron(II) Complexes and an Organic Photosensitizer. *Inorg. Chem.* **2021**, *60* (8), 5590−5597.
(56) Liu, J.; Goetjen, T. A.; Wang, Q.; Knapp, J. G.; Wasson, M. C.; Yang, Y.; Syed, Z. H.; Delferro, M.; Notestein, J. M.; Farha, O. K.; Hupp, J. T. MOF-Enabled Confinement and Related Effects for Chemical Catalyst Presentation and Utilization. *Chem. Soc. Rev.* **2022**, *51* (3), 1045−1097.
(57) Grissom, T. G.; Driscoll, D. M.; Troya, D.; Sapienza, N. S.; Usov, P. M.; Morris, A. J.; Morris, J. R. Molecular-Level Insight into CO_2 Adsorption on the Zirconium-Based Metal−Organic Framework, UiO-66: A Combined Spectroscopic and Computational Approach. *J. Phys. Chem. C* **2019**, *123* (22), 13731−13738.
(58) Benseghir, Y.; Solé-Daura, A.; Cairnie, D. R.; Robinson, A. L.; Duguet, M.; Mialane, P.; Gairola, P.; Gomez-Mingot, M.; Fontecave, M.; Iovan, D.; Bonnett, B.; Morris, A. J.; Dolbecq, A.; Mellot-Draznieks, C. Unveiling the Mechanism of the Photocatalytic Reduction of CO_2 to Formate Promoted by Porphyrinic Zr-Based Metal−Organic Frameworks. *J. Mater. Chem. A* **2022**, *10* (35), 18103−18115.
(59) Kajiwara, T.; Fujii, M.; Tsujimoto, M.; Kobayashi, K.; Higuchi, M.; Tanaka, K.; Kitagawa, S. Photochemical Reduction of Low Concentrations of CO_2 in a Porous Coordination Polymer with a Ruthenium(II)−CO Complex. *Angew. Chem., Int. Ed.* **2016**, *55* (8), 2697−2700.
(60) Zheng, X.; Drummer, M. C.; He, H.; Rayder, T. M.; Niklas, J.; Weingartz, N. P.; Bolotin, I. L.; Singh, V.; Kramar, B. V.; Chen, L. X.; Hupp, J. T.; Poluektov, O. G.; Farha, O. K.; Zapol, P.; Glusac, K. D. Photoreactive Carbon Dioxide Capture by a Zirconium−Nanographene Metal−Organic Framework. *J. Phys. Chem. Lett.* **2023**, *14* (18), 4334−4341.
(61) Creutz, C.; Chou, M. H.; Hou, H.; Muckerman, J. T. Hydride Ion Transfer from Ruthenium(II) Complexes in Water: Kinetics and Mechanism. *Inorg. Chem.* **2010**, *49* (21), 9809−9822.
(62) Huang, D.; Makhlynets, O. V.; Tan, L. L.; Lee, S. C.; Rybak-Akimova, E. V.; Holm, R. H. Fast Carbon Dioxide Fixation by 2,6-Pyridinedicarboxamidato-Nickel(II)-Hydroxide Complexes: Influence of Changes in Reactive Site Environment on Reaction Rates. *Inorg. Chem.* **2011**, *50* (20), 10070−10081.
(63) Jin, C.; Zhang, S.; Zhang, Z.; Chen, Y. Mimic Carbonic Anhydrase Using Metal−Organic Frameworks for CO_2 Capture and Conversion. *Inorg. Chem.* **2018**, *57* (4), 2169−2174.
(64) Heimann, J. E.; Bernskoetter, W. H.; Guthrie, J. A.; Hazari, N.; Mayer, J. M. Effect of Nucleophilicity on the Kinetics of CO_2 Insertion into Pincer-Supported Nickel Complexes. *Organometallics* **2018**, *37* (21), 3649−3653.

https://doi.org/10.1021/acs.inorgchem.5c02600
Inorg. Chem. 2025, 64, 18304−18315

(65) Bien, C. E.; Chen, K. K.; Chien, S.-C.; Reiner, B. R.; Lin, L.-C.; Wade, C. R.; Ho, W. S. W. Bioinspired Metal−Organic Framework for Trace CO_2 Capture. *J. Am. Chem. Soc.* **2018**, *140* (40), 12662−12666.

https://doi.org/10.1021/acs.inorgchem.5c02600
Inorg. Chem. 2025, 64, 18304−18315